Res Chem Intermed (2014) 40:2303–2313
DOI 10.1007/s11164-014-1607-8

Theory for optical assembling of anisotropic nanoparticles by tailored light fields under thermal fluctuations

Mamoru Tamura · Syoji Ito · Shiho Tokonami · Takuya Iida

Received: 22 January 2014 / Accepted: 15 February 2014 / Published online: 30 March 2014

Abstract In order to evaluate the assembling processes of arbitrary-shaped nanoparticles (NPs) by the irradiation of a tailored laser beam under thermal fluctuations, we have developed a "Light-induced-force Nano Metropolis Method (LNMM)" as a new theoretical method based on the stochastic algorithm in the energy region and the general formula of light-induced force. By using LNMM, we have investigated the change of configurations of silver NPs with anisotropic shapes under the irradiation of laser beams with various polarizations and intensity distributions (Gaussian beam and axially-symmetric vector beams) in an aqueous solution at room temperature. As a result, it has been clarified that silver NPs can be selectively arranged into a characteristic spatial configuration reflecting the properties of an irradiated laser beam (wavelength, intensity distribution, and polarization distribution), and that the assembled structures possess broadband spectra and exhibit a strong optical response to the irradiated laser beam through the optimization with the help of fluctuations.

M. Tamura · S. Tokonami · T. Iida (✉)
Nanoscience and Nanotechnology Research Center, Research Organization for the 21st Century, Osaka Prefecture University, 1-2, Gakuencho, Nakaku, Sakai, Osaka 599-8570, Japan
e-mail: t-iida@21c.osakafu-u.ac.jp

M. Tamura
Graduate School of Engineering, Osaka Prefecture University, 1-1, Gakuencho, Nakaku, Sakai, Osaka 599-8531, Japan

S. Ito
Division of Frontier Materials Science, Graduate School of Engineering Science, Osaka University, Toyonaka, Osaka 560-8531, Japan

S. Ito
Center for Quantum Science and Technology under Extreme Conditions, Osaka University, Toyonaka, Osaka 560-8531, Japan

Keywords Silver nanoparticle · Plasmon · Optical tweezers · Fluctuation · Simulation

Introduction

Many researchers have been trying bottom–up fabrication of functional structures based on self-assembling of nanomaterials with the help of fluctuations and dissipation [1]. Paying attention to the natural nanosystems, various functional biological systems have been constructed through evolution processes based on self-assembling; for example, DNA produces a variety of morphologies [2], a biomolecular motor exhibits efficient transport phenomenon [3], and a light harvesting antenna consisting of circularly arranged dye molecules provides high optical energy conversion rate [4]. In such an assembling process of functional nanosystems, it is considered that external perturbations played important roles in modulating the dissipation processes to obtain the optimized functions for the given environment.

On the other hand, light-induced force (LIF) that is used in optical tweezers [5] can be used as an external perturbation to control the dissipation and inter-object interaction [6, 7] during the assembling processes of nanoparticles (NPs). Metallic NPs are promising as the target material since they show a strong optical response that can overcome the thermal perturbation in liquid at room temperature, owing to the localized surface plasmon resonance (LSPR) depending on their shapes and sizes [8–11]. Recently, a theoretical method, the "light-induced-force nano dynamics method (LNDM)", was developed to evaluate the dynamics of NPs under light irradiation and thermal fluctuations in the time domain [12]. By using LNDM, it was clarified that LSPR in densely assembled metallic NPs shows the prominent red-shift and spectral broadening due to the *plasmonic superradiance* depending on their spatial configuration, and a similar phenomenon was experimentally observed in densely assembled Au NPs on a plastic microbead [13]. Thanks to these interesting optical properties, metallic NPs are applied to various research fields, for example, biosensors in the field of analytical chemistry [14, 15], where a homogenization of shapes and sizes becomes an important subject in order to obtain a high performance. There are several reports on sorting methods of NPs using LIF, for example, the utilization of the size-sensitivity of resonant wavelength of quantum dots under a cryogenic condition [16, 17], and the utilization of the difference of transport properties of NPs depending on their sizes under the fluctuations and intensity-modulated light standing wave [18]. In the recent past, we experimentally demonstrated for the selective extraction of Ag NPs with uniform shape and size under thermal fluctuations even at room temperature, and simultaneously assembled the NPs into a particular configuration reflecting the properties of irradiated light [19].

In this paper, in order to analyze the detailed mechanism of such a selective assembling of metallic NPs under fluctuations, we develop a novel calculation method, the "*Light-induced-force Nano Metropolis Method* (LNMM)" in the energy region that is complementary with LNDM, and show the mechanism of the optimization of their optical spectrum for an irradiated light. In particular, as an application of LNMM, we have evaluated the assembling process of NPs focusing

on the Gaussian beam and the doughnut beams with the ring-like intensity distributions and the axially symmetric polarizations as irradiated light fields.

Theory and model

Development of "Light-induced-force Nano Metropolis Method (LNMM)"

In order to evaluate the assembling processes of NPs under the laser beams with designed properties and fluctuations, we have developed a theoretical method, i.e., LNMM, to search energetically stable or metastable configurations, which is based on the general expression of LIF for materials from macroscopic to microscopic scales [6, 7], and the Metropolis method with a stochastic algorithm. The general expression of LIF is given by the following form,

$$\mathbf{F}_{\mathrm{LIF}} = \frac{1}{2}\mathrm{Re}\left[\sum_{\omega}\int_{V} d\mathbf{r}(\nabla\mathbf{E}(\mathbf{r},\omega)^{*})\cdot\mathbf{P}(\mathbf{r},\omega)\right], \tag{1}$$

where $\mathbf{E}$ is the response field and $\mathbf{P}$ is the induced polarization. Here, we divide the NPs into multiple cells to express anisotropy of NPs, where the total number of cells is N_{cells}. Based on the discrete dipole approximation [20], we can self-consistently obtain $\mathbf{E}$ and $\mathbf{P}$ by solving the following simultaneous equations,

$$\mathbf{E}_i = \mathbf{E}_i^{(0)} + \sum_{j\neq i}^{N_{\mathrm{cells}}} \mathbf{G}_{i,j}\cdot\mathbf{P}_j V_j + S_i\mathbf{P}_i \tag{2}$$

$$\mathbf{P}_j = \chi_j\mathbf{E}_j, \tag{3}$$

where $\mathbf{E}_i^{(0)}$ is the incident electric field, V_j is the volume of each cell, $\mathbf{G}_{i,j}$ is a Green's function in the homogeneous medium, S_i is the analytical integral of Green's function (self-term) in each cell corresponding to the case of $i = j$ in Eq. (3), and χ_j is the electric susceptibility near the visible light region given by the Drude model.

The NPs are driven by LIF and show the stochastic behavior due to the fluctuations in liquid medium. We can investigate these metastable states by random spatial displacement of NPs based on the Metropolis algorithm as follows. In each step, NPs are randomly moved according to the next transition probability,

$$p = \min[1, \exp(-\Delta H/k_{\mathrm{B}}T)] \tag{4}$$

$$\Delta H = -\sum_{i}^{N_{\mathrm{cells}}} \mathbf{F}_i\cdot\Delta\mathbf{r}_i + \Delta V_{\mathrm{DLVO}}, \tag{5}$$

where ΔH is the potential change of the total system before and after the random motion given by the LIF and DLVO theory [21]. Equation (4) means that a result of random displacement is employed or rejected according to the probability of $\exp(-\Delta H/k_{\mathrm{B}}T)$ when the system is more unstable with higher energy ($\Delta H > 0$), and that the displacement is employed with $p = 1$ when the system is more stable

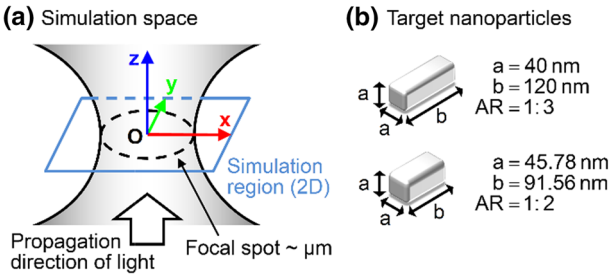

Fig. 1 Assumed model for the calculation

with lower energy ($\Delta H < 0$). From a particular initial configuration of NPs, by repeating the above process (we employ 10^6 steps in this paper), we can finally obtain the stable configuration.

Model of target anisotropic NPs and laser beams

Figure 1 shows the simulation model. We assume the situation that Ag NPs are dispersed in the water at room temperature (298 K) and irradiated with incident light. However, for the essential discussion, we have performed the simulation in a two-dimensional system, and the target NPs move only on the x–y plane (Fig. 1a). Incident light is propagating along the z-axis and the focal point is set at the origin. As a simulation target, two types of anisotropic Ag NPs of rectangular cylinders with almost the same volume but different aspect ratios (AR) are assumed. The sizes of a NP with high-aspect ratio and a NP with low-aspect ratio are 40 × 120 nm and 45.78 × 91.56 nm with 1:3 and 1:2 in AR, respectively. We perform the simulation under the condition that only respective types of NPs are initially configured in a square lattice of 7 × 7 within -1 μm $< x, y <$ 1 μm.

For the irradiated beams shown in Fig. 2, we employ three types of laser beams, i.e., the Gaussian beam and the doughnut beams with the radial and azimuthal polarizations [22, 23]. The wavelength of each beam is set to 1,064 or 660 nm. We assume an input laser power of 25 mW, and the maximum intensity of the azimuthal beam is approximately 147 kW/cm^2, which is located at ±1 μm from the optical axis. The spatial distribution of the Gaussian beam is is given in Fig. 1a (the intensity becomes 1/e^2 at 2.33 μm from the optical axis) which gives the same maximum intensity as those of the azimuthal beam and the radial beam as shown in Fig. 1d. Due to the z-component of the focused radial beam, its intensity distribution is slightly higher than that of the azimuthal beam but the difference has little influence under the present condition. These distributions are calculated for the 1,064-nm beam wavelength, whereas almost the same distribution is assumed for the 660-nm beam wavelength.

Calculation of scattering spectra

In order to evaluate the scattering spectra of NPs before and after the optical assembling, we assume the plane wave incident light $\mathbf{E}_i^{(0)} = \vec{\eta} E^{(0)} \exp[i\mathbf{k} \cdot \mathbf{r}_i]$, where

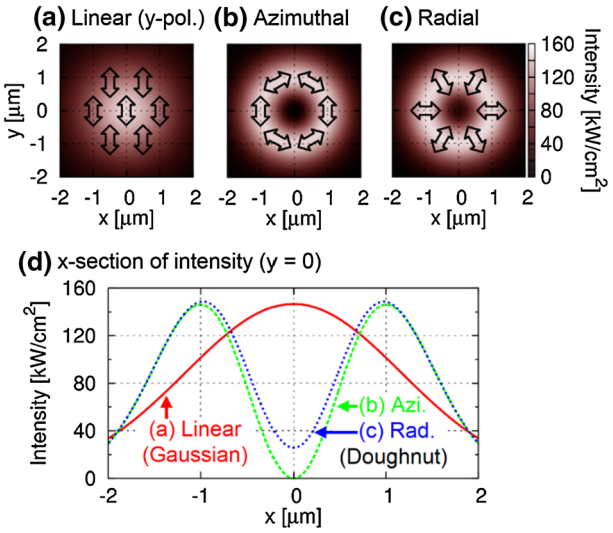

Fig. 2 As an incident light, we employ **a** the Gaussian beam with the linear (y) polarization, and the doughnut beams with **b** the azimuthal and **c** the radial polarization. The density plot as the background shows the intensity distribution of the beams. Respective polarization directions are indicated by the *double-headed arrows*. **d** The intensity distribution of respective beams in x-direction for $y = 0$

$\vec{\eta}$ is the unit vector of polarization direction, $E^{(0)}$ is the amplitude of incident light, and **k** is the wave number as the vector of light propagating direction. Under the irradiation of this light, we can evaluate the extinction cross-section σ_{ext} proportional to the LIF exerted on the NPs. And we can evaluate the absorption cross-section σ_{abs} from the equation of Joule heat defined as $W = V\langle \mathbf{J} \cdot \mathbf{E} \rangle$ and relationship between the electric current **J** and the polarization **P**. Thus, we can evaluate the scattering cross-section with the relationship $\sigma_{\text{scat}} = \sigma_{\text{ext}} - \sigma_{\text{abs}}$ [7]. Especially, the scattering spectra for the incident light with the various polarization directions are important because the results shown later have the axial symmetric configuration. In order to understand the effect of this axial symmetry, we evaluate the average scattering spectra $\langle \sigma_{\text{scat}} \rangle_{\text{rot}}$ for the directions of unit vector $\vec{\eta}$ by the following equation,

$$\langle \sigma_{\text{scat}} \rangle_{\text{rot}} = \frac{1}{n} \sum_{i=0}^{n-1} \sigma_{\text{scat}} \left(\vec{\eta} = \left(\cos \frac{i\pi}{n}, \sin \frac{i\pi}{n}, 0 \right) \right), \tag{6}$$

where we assume $n = 180$ to evaluate the rotational average in steps of 1-degree.

Results and discussion

In order to discuss the essential effects of LIF on the assembling of NPs, we calculate the LIF exerted on NPs under the irradiation of the simple Gaussian beam of 1,064 nm wavelength and y-polarization (Fig. 3). When only the NP_1 is present,

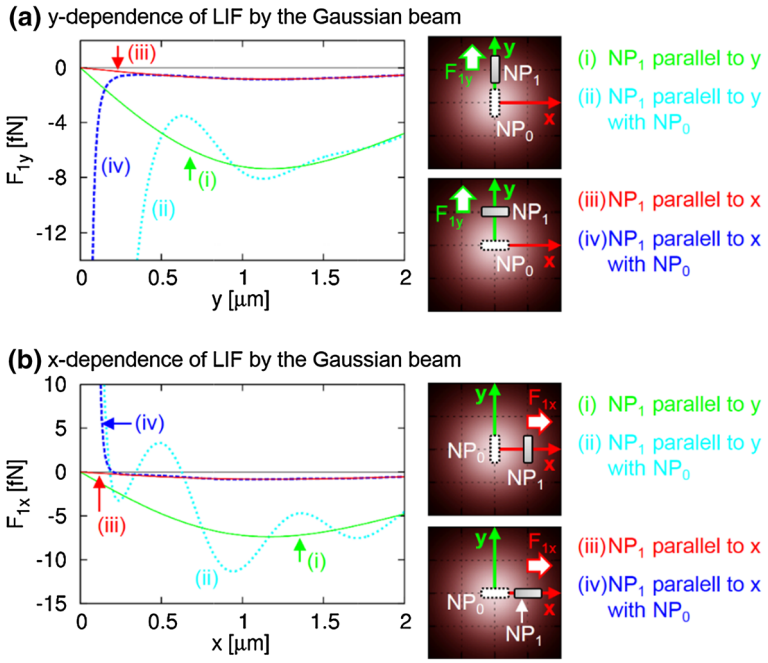

Fig. 3 **a** *y*-dependence and **b** *x*-dependence of LIF by the *y*-polarized Gaussian beam. The LIF exerts on NP_1 change according to the direction of NP_1 and the presence or absence of NP_0. NP_1 is parallel to the *y*-axis and *x*-axis in (i), (ii) and (iii), (iv), respectively. NP_0 is absent and present in (i), (iii) and (ii), (iv), respectively. (Color figure online)

the NP_1 is trapped by the gradient force as the component of LIF. The gradient force depends on an intensity gradient and the direction can be changed with light wavelength. When light wavelength is longer (shorter) than LSPR wavelength, i.e., red-detuned (blue-detuned), a NP is attracted into the high (low) intensity region. Therefore, the direction of NP_1 causes the large change of the gradient force, because the main peak of LSPR of the longitudinal axis of NP exists near 800 nm as shown in Figs. 4, 5 and 6, and are excited by the light of 1,064 nm, whereas the LSPR of short axis exists near 400 nm and has a small peak value. When the NP_0 is located near NP_1, the inter-particle LIF arises between them. When NPs are separately placed, the inter-particle LIF becomes comparatively small and the gradient force contributes to the total LIF. However, when NPs are closely spaced, the inter-particle LIF becomes significantly strong. In this case, the strong attractive LIF arises between NPs when NPs are arranged in a polarization direction as shown in Fig. 3a, whereas the strong repulsive LIF arises when NPs are aligned in the direction perpendicular to the polarization as shown in Fig. 3b. Thus, under the irradiation of light of 1,064 nm wavelength, NPs are arranged and coupled along the direction of a light polarization with a certain disorder arising from the thermal fluctuations from the surrounding medium.

The main results about the optical assembling of NPs are shown for laser beams with different types of spatial distributions (Figs. 4, 5, 6). The results in the case of

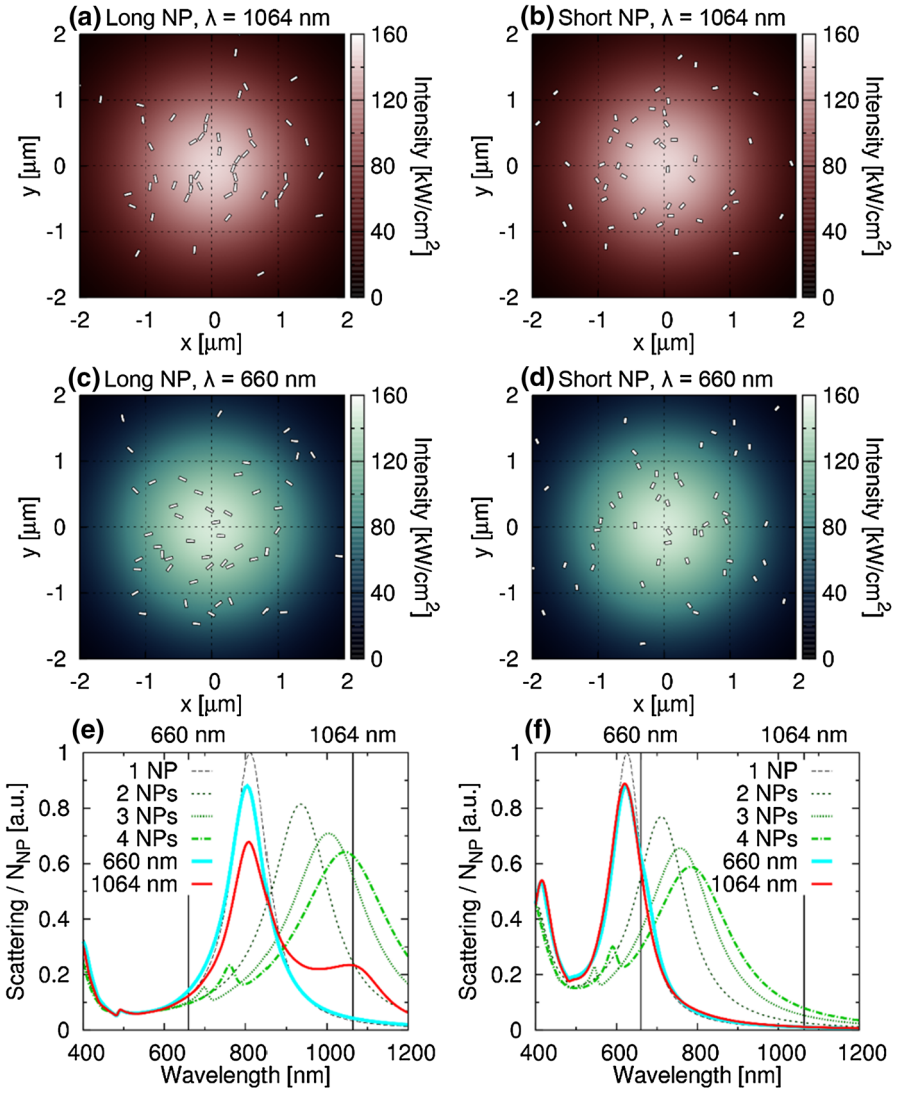

Fig. 4 Results of LNMM simulation and average scattering spectra obtained at the final configuration (after 10^6 steps) of 49 long and short NPs, respectively, in the case of **a**, **b** 1,064 nm and **c**, **d** 660 nm in wavelength. In addition, **a**, **c** the long NPs and **b**, **d** the short NPs are assumed. **e**, **f** show the rotational average of scattering spectra after irradiation of 660 nm (*watery line*) and 1,064 nm (*red line*) beams for long NPs and short NPs, respectively. Graph legends, *1 NP* and *2–4 NPs*, show the averaged scattering spectra of single NP and 2–4 NPs with 30 nm of inter-particle distance in the direction of longitudinal axis. The *vertical lines* show 660 and 1,064 nm wavelengths. (Color figure online)

the Gaussian beam with 1,064 nm and 660 nm wavelengths are shown for NPs with different ARs, respectively (Fig. 4). In each case, the NPs are optically trapped near the high intensity region, and the NPs are orientated parallel to the light polarization in Fig. 4a, d. However, in Fig. 4c, the NPs are orientated in a direction

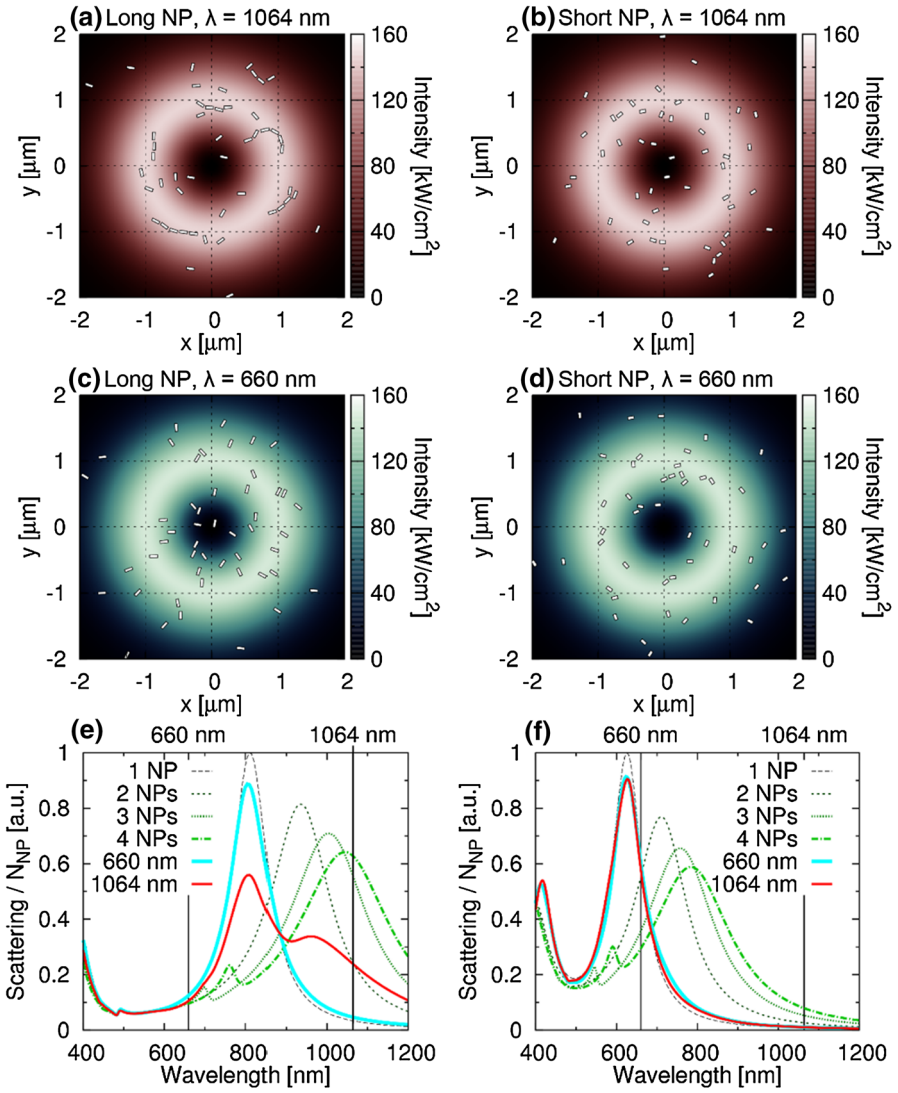

Fig. 5 Results in the case of the azimuthal beam under the same conditions as Fig. 4 except for the polarization. (Color figure online)

perpendicular to the light polarization since the 660 nm wavelength is the red-detuned for the short axis LSPR and the gradient force due to the short axis mode is stronger than that due to the long axis mode. As for Fig. 4b, 1,064 nm in wavelength is far from the LSPR peaks of the long and short axis of the short NPs, thus NPs are exerting weak LIF on, and randomly orientated with, large separation. As the more characteristic point, in Fig. 4a, we can confirm the electromagnetically coupled NPs with small separations due to the attractive inter-particle LIF parallel

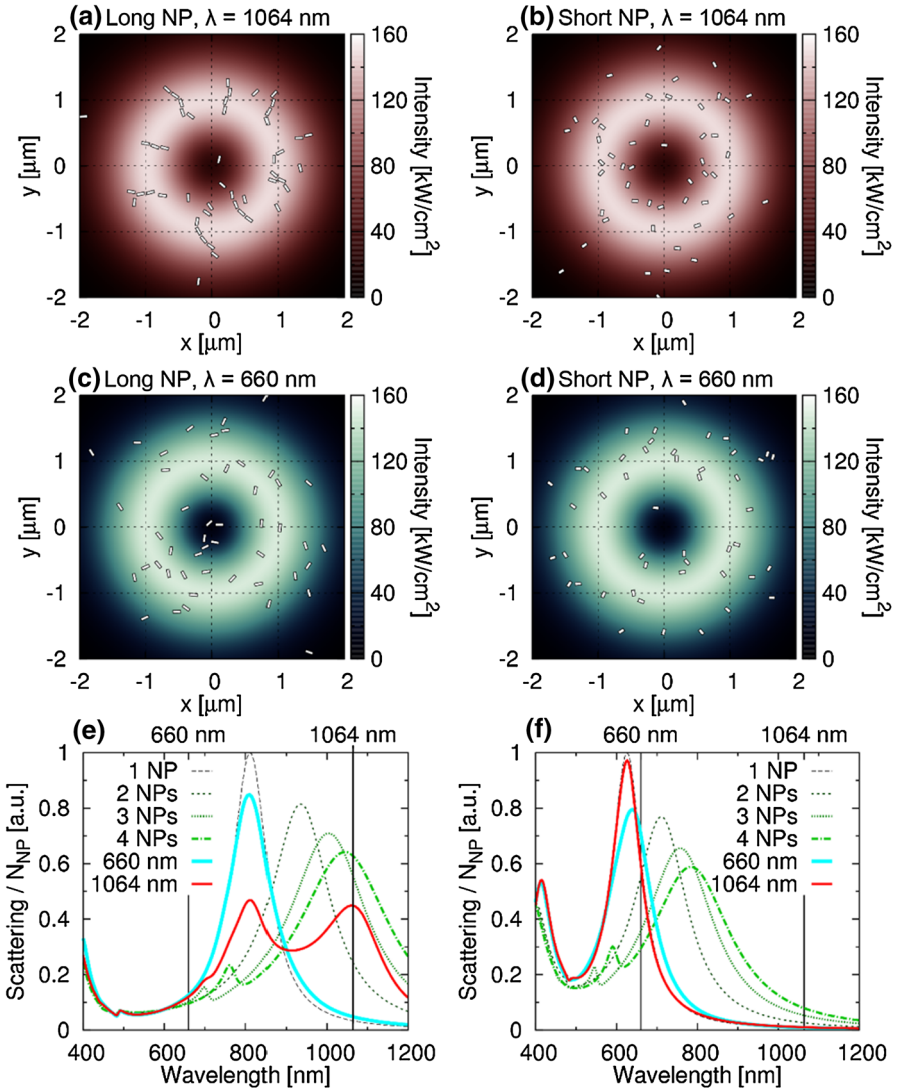

Fig. 6 Results in the case of the radial beam under the same conditions as Fig. 4 except for the polarization. (Color figure online)

to the polarization. Such a coupling of the NPs leads to large red-shift and spectral broadening due to the *plasmonic suparradiance* [12], as shown in Fig. 4e. Also, there are closely-spaced NPs in Fig. 4b, d, but coupling is weak under the present condition and their scattering spectrum is not modulated and almost similar to that of the single NP.

Next, Figs. 5 and 6 are the results in the case of the doughnut beams of the azimuthal and radial polarizations, respectively. Similar to the results in Fig. 4, the NPs are

attracted into the high intensity region and orientated parallel or perpendicular to the polarization of the light. Additionally, the NPs confined in a doughnut-shaped intensity region, electromagnetically interact with each other according to the axially symmetric polarization, and are assembled into a characteristic spatial configuration reflecting the properties of irradiated light. These structures can respond to a broadband light with various polarization directions like sunlight, and the potential application of tunable white light scattering. For example, in Fig. 6e, the scattering spectrum at the configuration of Fig. 6a after 1,064 nm beam irradiation is clearly broadened and shifted because the NPs are strongly coupled under the attractive interaction with small separation in the radial direction. In the case of the azimuthal polarization of Fig. 5a, the clusters of the coupled NPs show unique bending to decrease the interaction energy under the azimuthal polarization, where the gradient force is inverted under blue-detuned condition due to the large red-shift of LSPR, and the repulsive inter-object LIF also arises between the clusters. On the other hand, in Fig. 6a, the clusters are also bent, but the repulsive interaction between the clusters perpendicular to the radial polarization creates a stabilized configuration with a certain type of order. Thus, we can see a comparatively large red-shift in scattering spectra under the radial polarization. Similarly, in Fig. 6d, some NPs are coupled and so the scattering spectrum is slightly shifted.

Additionally, the dissipative force as one of the LIF, which is caused by the absorption and the scattering processes, can push NPs along the propagation direction of the light. According to the scattering spectra in Figs. 4, 5 and 6, the long and short NPs are selectively pushed by such a dissipative force under the tuned LSPR for the irradiated wavelength. Thus, we can expect that the long and short NPs are selectively transported from the mixtures of inhomogeneous NPs under the irradiation of the light with 1,064 and 660 nm wavelengths, respectively. Especially, the arrangements of the long NPs, which have the significantly red-shifted LSPR peak, are pushed by the strong dissipative forces and accelerate the selective assembling. In fact, the experimental results in Ref. [19] showed the sensitive dependence on the light wavelength, and the different NPs were deposited on the substrate even after a washing of the substrate. These facts mean the possibility of selective assembling of the desired NPs by arbitrarily designed laser beams with various properties.

Summary and prospects

We have developed a new simulation method, LNMM, to investigate the assembling process of the anisotropic NPs under the designed laser irradiation and the fluctuations. As an application of LNMM, we treated the model system consisting of Ag NPs in aqueous solution assuming the Gaussian beam and the doughnut beams with axially-symmetric polarizations as irradiated beams, where we clarified the detailed mechanism of selective assembling under thermal fluctuations. Such theoretical results indicate that laser beams with different wavelengths will enable us to extract NPs with uniform size, shape, and the characteristic spectrum property of the obtained structures. Additionally, the light

intensity distribution contributes to the sketch of spatial configuration of assembled NPs, and the polarization distribution of the irradiated light contributes to the orientations. In this manner, we can obtain the characteristic assembled structure of Ag NPs. In addition to the axially-symmetric polarizations used in this paper, the recent optical technologies enable us to realize the holographic optical tweezers for the three-dimensional manipulation, and to generate another type of doughnut beam such as the Laguerre-Gaussian beam with the orbital angular momentum. The combination of these advanced laser techniques would provide more complex configurations with unconventional optical functions. In the future, our clarified optical assembling mechanism will provide a promising avenue for the bottom–up creation of various useful nanocomposite materials with high optical energy conversion efficiency, microstructures exhibiting sensitive response to the attachment of biological molecules, and so on.

Acknowledgments The authors would like to thank Prof. T. Tsutsui, Prof. H. Ishihara, and Prof. H. Miyasaka for kind encouragement and support. Also, they thank Mr. S. Hidaka, Mr. H. Hattori, Dr. H. Yamauchi, Mr. Nishida, and Dr. T. Itoh for their fruitful discussion. This work was supported by PRESTO from the JST; a Grant-in-Aid for Scientific Research (B) No. 23310079; a Grant-in-Aid for Young Scientists (A) No. 23681023; the Grants-in-Aid for Exploratory Research No. 23655072 and No. 24654091 from the JSPS; and Special Coordination Funds for Promoting Science and Technology from the MEXT (Improvement of Research Environment for Young Researchers (FY 2008–2012).

References

1. E. Rabani, D.R. Reichman, P.L. Geissler, L.E. Brus, Nature **426**, 271 (2003)
2. P.W.K. Rothemund, Nature **440**, 297 (2006)
3. N. Kodera, D. Yamamoto, R. Ishikawa, T. Ando, Nature **468**, 72 (2010)
4. S. Scheuring, J.N. Sturgis, Science **309**, 484 (2005)
5. A. Ashkin, J.M. Dziedzic, J.E. Bjorkholm, S. Chu, Opt. Lett. **11**, 288 (1986)
6. T. Iida, H. Ishihara, Phys. Rev. Lett. **97**, 117402 (2006)
7. T. Iida, H. Ishihara, Phys. Rev. B **77**, 245319 (2008)
8. F. Hao, C.L. Nehl, J.H. Hafner, P. Nordlander, Nano Lett. **7**, 729 (2007)
9. S. Zhang, K. Bao, N.J. Halas, H. Xu, P. Nordlander, Nano Lett. **11**, 1657 (2011)
10. L.J. Sherry, S.-H. Chang, G.C. Schatz, R.P. Van Duyne, B.J. Wiley, Y. Xia, Nano Lett. **5**, 2034 (2005)
11. L.J. Sherry, R. Jin, C.A. Mirkin, G.C. Schatz, R.P. Van Duyne, Nano Lett. **6**, 2060 (2006)
12. T. Iida, J. Phys. Chem. Lett. **3**, 332 (2012)
13. S. Tokonami, S. Hidaka, K. Nishida, Y. Yamamoto, H. Nakao, T. Iida, J. Phys. Chem. C **117**, 15247 (2013)
14. S. Tokonami, Y. Yamamoto, H. Shiigi, T. Nagaoka, Anal. Chim. Acta **716**, 76 (2012)
15. J. Mitchell, Sensors **10**, 7323 (2010)
16. T. Iida, H. Ishihara, Phys. Rev. Lett. **90**, 057403 (2003)
17. K. Inaba, K. Imaizumi, K. Katayama, M. Ichimiya, M. Ashida, T. Iida, H. Ishihara, T. Itoh, Phys. Status Solidi B **243**, 3829 (2006)
18. M. Tamura, T. Iida, Nano Lett. **12**, 5337 (2012)
19. S. Ito, H. Yamauchi, M. Tamura, S. Hidaka, H. Hattori, T. Hamada, K. Nishida, S. Tokonami, T. Itoh, H. Miyasaka, T. Iida, *Sci. Rep.*, 3047 (2013)
20. O.J.F. Martin, N.B. Piller, Phys. Rev. E **58**, 3909 (1998)
21. T. Kim, K. Lee, M. Gong, S.-W. Joo, Langmuir **21**, 9524 (2005)
22. R. Oron, S. Blit, N. Davidson, A.A. Friesem, Z. Bomzon, E. Hasman, Appl. Phys. Lett. **77**, 3322 (2000)
23. B. Gu, Y. Cui, Opt. Exp. **20**, 17684 (2012)